ENVIRONMENTAL RESEARCH
LETTERS

LETTER • OPEN ACCESS

# Unprecedented Arctic sea ice thickness loss and multiyear-ice volume export through Fram Strait during 2010–2011

To cite this article: Xuewei Li *et al* 2022 *Environ. Res. Lett.* **17** 095008

IOP Publishing Environ. Res. Lett. 17 (2022) 095008 https://doi.org/10.1088/1748-9326/ac8be7

ENVIRONMENTAL RESEARCH
LETTERS



OPEN ACCESS

RECEIVED
24 February 2022

REVISED
18 August 2022

ACCEPTED FOR PUBLICATION
23 August 2022

PUBLISHED
1 September 2022



LETTER

# Unprecedented Arctic sea ice thickness loss and multiyear-ice volume export through Fram Strait during 2010–2011

**Xuewei Li[1], Qinghua Yang[1,*], Lejiang Yu[2], Paul R Holland[3], Chao Min[1], Longjiang Mu[4] and Dake Chen[1]**

[1] School of Atmospheric Sciences, Sun Yat-sen University, and Southern Marine Science and Engineering Guangdong Laboratory, Zhuhai 519082, People's Republic of China
[2] MNR Key Laboratory for Polar Science, Polar Research Institute of China, Shanghai 200136, People's Republic of China
[3] British Antarctic Survey, Cambridge CB3 0ET, United Kingdom
[4] Pilot National Laboratory for Marine Science and Technology, Qingdao 266237, People's Republic of China
* Author to whom any correspondence should be addressed.

**E-mail:** yangqh25@mail.sysu.edu.cn

**Keywords:** Arctic, sea ice thickness, thermodynamics, dynamics

Supplementary material for this article is available online

## Abstract

The satellite-observed sea ice thickness (SIT) records from 2003 to 2020 identify an extreme SIT loss during 2010–2011. Ice thickness budget analysis demonstrates that the thickness loss was associated with an extraordinarily large multiyear ice (MYI) volume export through the Fram Strait during the season of sea ice advance. High cloudiness led to positive anomalies of net longwave radiation, and positive net surface energy flux anomalies supported enhanced sea ice melt from June to August. Due to the MYI loss, the Arctic sea ice became more sensitive to subsequent atmospheric anomalies. The reduced surface albedo triggering a positive ice-albedo amplifying feedback and contributed to the accelerating loss of ice thickness. These tightly coupled events highlight that the increasingly younger and thinner Arctic sea ice is becoming more vulnerable to external forcing and created the precondition for the rapid reduction in sea ice extent in 2012.

## 1. Introduction

Arctic sea ice plays an important role in the climate system. The exchanges of moisture, heat and momentum between the atmosphere and the polar oceans are strongly influenced by ice thickness, particularly when the ice is thin. The thinning of Arctic sea ice well reflects recent climate changes. The submarine and satellite (Ice, Cloud, and land Elevation Satellite, ICESat) records reveal a long-term trend of Arctic sea ice thinning since 1958–2008 (Rothrock *et al* 2008, Kwok and Rothrock 2009). Min *et al* (2019) claimed that the minimum sea ice thickness (SIT) occurs in 2011, using a model combined with satellite thickness data, and this is also found in satellite data alone (Kwok and Cunningham 2015, Tilling *et al* 2015, Liu *et al* 2020). The seasonal evolution of mean Arctic SIT and sea ice volume (SIV) based on CS2SMOS dataset from October 2010 through April 2020 are contrasted in figures 1(g) and (h). The mean SIT within the area of actual ice coverage in October 2011 was strongly anomalous, so was the loss in multiyear ice (MYI) volume (figures 1(g) and (h)). Along with the observed decrease in SIT, MYI has been shrinking faster than the entire sea ice (Comiso 2002, Kwok and Untersteiner 2011). The fraction of MYI in the total ice extent in March decreased from about 75% in the mid 1980s to 45% in 2011 (Maslanik *et al* 2011). Most notably, younger and thinner ice becomes more sensitive to dynamic and thermodynamic effects such as ice drift and melting (McPhee *et al* 1998, Maslanik *et al* 2007a).

As the precondition for the rapid reduction in sea ice extent in 2012, perennial ice in 2011 was nearly as low as that in 2007, and MYI in the 2011–2012 winter season was a record low (Screen *et al* 2011, Parkinson and Comiso 2013, Zhang *et al* 2013). However, due to the lack of satellite-observed SIT in summer, little is known about how the ice thickness and ice age have changed from 2010 to 2011. To advance upon these existing studies, we use a well-validated daily SIT reanalysis data covering the melting season, applying

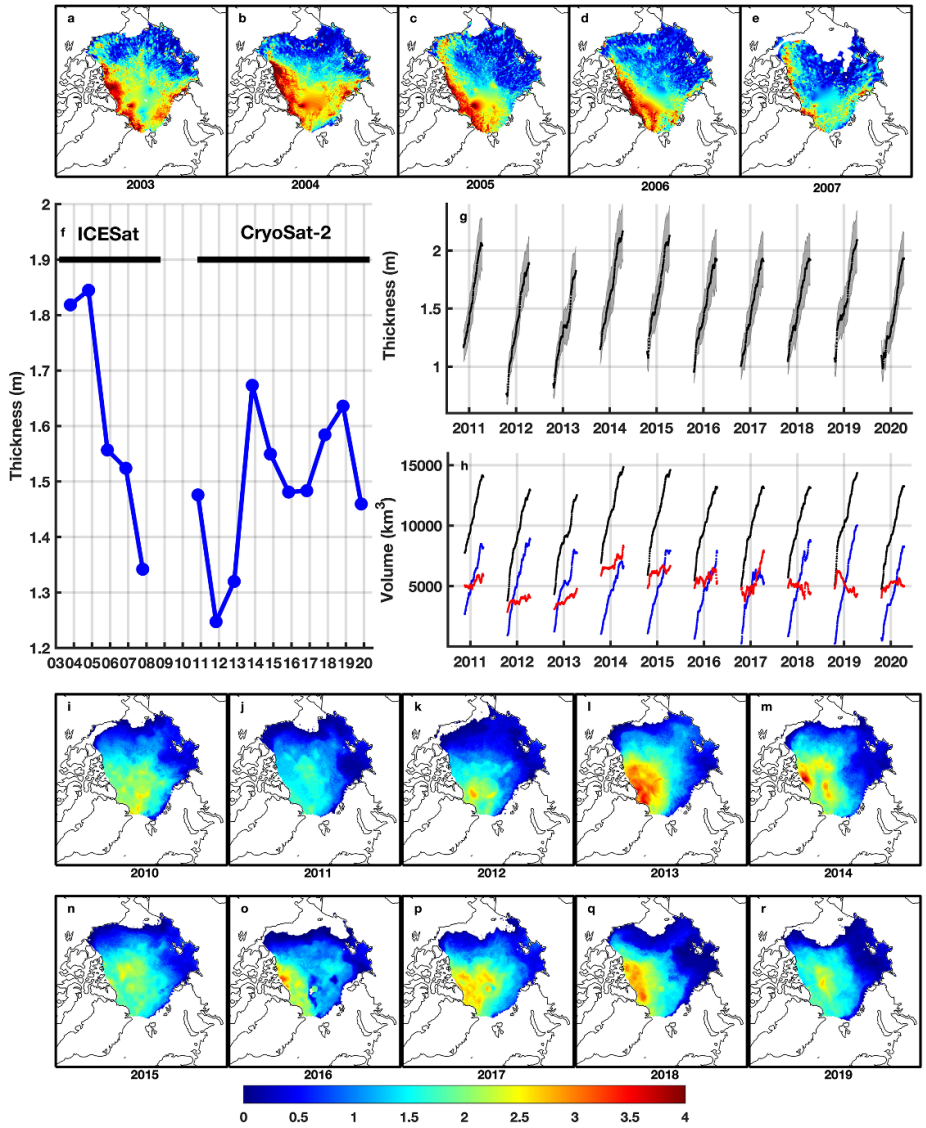


**Figure 1.** Interannual changes in fall sea ice thickness. (a)–(e) Spatial patterns of ice thickness in fall (October–November) based on the ICESat (2003–2007). (f) Interannual changes in fall sea ice thickness based on the ICESat (2003–2007) and CryoSat-2 (2010–2020) satellite datasets. (g) Daily behavior of mean sea ice thickness within area of actual ice coverage based on CS2SMOS dataset from October 2010 through April 2020. Gray shading shows the quality of CS2SMOS data. (h) Daily behavior of total(black), first-year(blue) and multiyear (red) sea ice volumes within Arctic basin based on CS2SMOS dataset from October 2010 through April 2020. (i)–(r) Spatial patterns of ice thickness in fall (October–November) based on the CryoSat-2 (2010–2020). Arctic basin mean sea ice thickness is computed within the bounded by the gateways into the Pacific (Bering Strait), the Canadian Arctic Archipelago, and the Greenland (Fram Strait) and Barents Seas.

SIT budgets to further investigate the dynamic and thermodynamic mechanisms involved in the SIT anomaly in fall 2011. In this study, we address two major questions by sea ice budget analysis. First, what special factors led to the precipitous decrease of SIT in 2011? Second, are the changes predominantly dynamic or thermodynamic in origin? The paper is organized as follows: section 2 describes the observations and model data used in this study and presents the methods that we employed to investigate the sea ice budgets. In section 3, we evaluate the sea ice budget anomalies in 2011. Moreover, the mechanism for sea ice thinning in response to the driving climatic factors are described. We summarize and discuss the major findings of this study in section 4.

## 2. Data and methods

The evolution of SIT is governed by the dynamic and thermodynamic processes. The thickness can be separated by a simple conservation equation (Bitz *et al* 2005, Holland *et al* 2014)

$$\frac{\partial H}{\partial t} = -\nabla \cdot (uH) + \text{residual}, \tag{1}$$

$$= -u \cdot \nabla H - H\nabla \cdot u + \text{residual} \tag{2}$$

where $H$ is SIT and $u$ is ice motion. The term on the left-hand side $\frac{\partial H}{\partial t}$ is referred to as ice 'thickening', which is determined by ice thickness

flux divergence, $\nabla \cdot (uH)$ and the residual. The flux divergence can be separated into 'advection', $u \cdot \nabla H$, and 'divergence', $H\nabla \cdot u$. The residual represents the thermodynamic melting and freezing. We adopt the sign convention that positive values of all terms are associated with an increase in ice thickness. In a related approach, Holland and Kimura (2016) examine the Arctic ice concentration budget terms, which is highly instructive, but our purpose is to assess the ice thickness budget. The SIT is defined as grid cell-averaged ice thickness, which is also called effective ice thickness. The effective ice thickness is the product of the average ice thickness and the ice area concentration and equals the volume of ice per unit area of ocean.

We apply this methodology to a well-validated SIT and drift dataset (the combined model and satellite thickness data, CMST), which was generated by the MITgcm ice-ocean model with CryoSat2, the soil moisture and ocean salinity (SMOS) SIT and the satellite sensors Special Sensor Microwave Imager/-Sounder (SSMIS) sea ice concentration assimilated (Mu *et al* 2018). The CMST thickness data cover both the cold seasons and the melting seasons for the period of October 2010 to December 2016 on an 18 km grid. The CMST has been already quantitatively evaluated against observations by a previous study (Mu *et al* 2018, Min *et al* 2019), demonstrating an accurate performance in simulating the real sea ice drift and thickness. To reduce the noise in ice drift fields and hence divergence calculation, we follow Holland and Kimura (2016) and smooth ice drifts with a 400 × 400 km square-window filter.

To evaluate sea ice variability, we use the Arctic SIT and concentration data based on the European Space Agency (ESA) and the Alfred Wegener Institute (AWI) CryoSat-2 satellite (Ricker *et al* 2014, Kurtz and Harbeck 2017). The ESA ice thickness data are provided daily from October 2010 to April 2020, while the AWI ice thickness are provided weekly. We also use the weekly sea ice age for the Arctic Ocean (Tschudi *et al* 2020). The method used to estimate sea ice age involves Lagrangian tracking of sea ice from week-to-week using gridded ice motion vectors (Maslanik *et al* 2011, Tschudi *et al* 2020).

We also use the SIT and drift in CMST data to compute ice volume export through Fram Strait. We follow the previous definition of gate position and defined the gate at 82° N between 12° W and 20° E and 20° E between 80.5 and 82° N (Krumpen *et al* 2016, see supplementary figure S1). Because the EASE-Grid Sea Ice Age product is not provided near coasts, the sum of first-year ice (FYI) and MYI is slightly less than the total amount of ice.

In this study, to quantify the thermodynamic impact on the ice thickness budget, we estimate monthly sea level pressure (SLP), 10 m wind speed, surface radiation fluxes, and albedo anomalies, derived from the fifth generation European Centre for Medium-Range Weather Forecasts ReAnalysis product (ERA5) (Copernicus Climate Change Service (C3S) 2017, Hersbach *et al* 2020).

## 3. Results

### 3.1. SIT budget anomalies

Based on the CryoSat-2 satellite observations, from 20 October 2010 to 20 October 2011, the Arctic basin had lost more than 920 $km^3$ of ice volume, with the central Arctic accounting for 88% of the loss (figure 1). The CryoSat-2 satellite dataset showed that the Arctic basin mean SIT anomalies was 0.26 m below the average over 2010–2019. The CMST overestimated the sea ice thickess loss, but it well captured the general spatial pattern of the ice thickness loss, especially in the Central Arctic. Generally, the anomaly of the total sea ice thickening was negative in 2011, which indicated that more sea ice was being lost in the whole Arctic region, especially in the north of Canadian Arctic Archipelago (CAA) (figure 2). Notably, the Arctic Ocean had lost 809 $km^3$ of MYI from 2010 to 2011, accounting for 88% of the total sea ice loss. The total exported ice volume anomaly through the Fram Strait fluctuated little in 2010–2011, but about 40% of the MYI loss was directly due to the strengthened ice export at the Fram Strait.

To discriminate the sources for the SIT anomalies, we analyzed the Arctic SIT budget anomalies covering both the cold seasons and the melting seasons from 2010 to 2011 by subtracting the six year mean from each month (figure 2). According to the CMST, the total Arctic basin mean anomaly from 2010 to 2011 was 0.31 m. The thermodynamic ice loss played an important role. The residual was dominated by thermodynamics, with more ice thickness loss of 0.25 m, while the anomaly of total ice thickness divergence and advection was −0.05 m and −0.01 m, respectively. Correspondingly, the thermodynamic forcing and the sea ice divergence accounted for 81% and 16% of the ice thickness loss.

According to the timing of ice advance versus ice retreat, we time-integrated the Arctic SIT budget into seasonal means for the seasons of sea ice advance (October–April) and retreat (May–September). The Arctic sea ice thickening increased (declined) rapidly from October to April (May–September). During the season of sea ice advance, the thickening anomaly is relatively weak. The negative thickening anomaly (approximately −0.1 meters per month) appeared along the north of CAA and the coast of the East Siberian Sea (ESS). Most regions were subject of enhanced divergence, while increased convergence is indicated around the coast of the BS. Advection anomalies transported sea ice from BS, CS, and ESS to the Fram Strait along the CA coast, resulting in increased SIT north of Spitsbergen and the Fram Strait. Residual (thermodynamic) anomalies were relatively weak but matched the overall

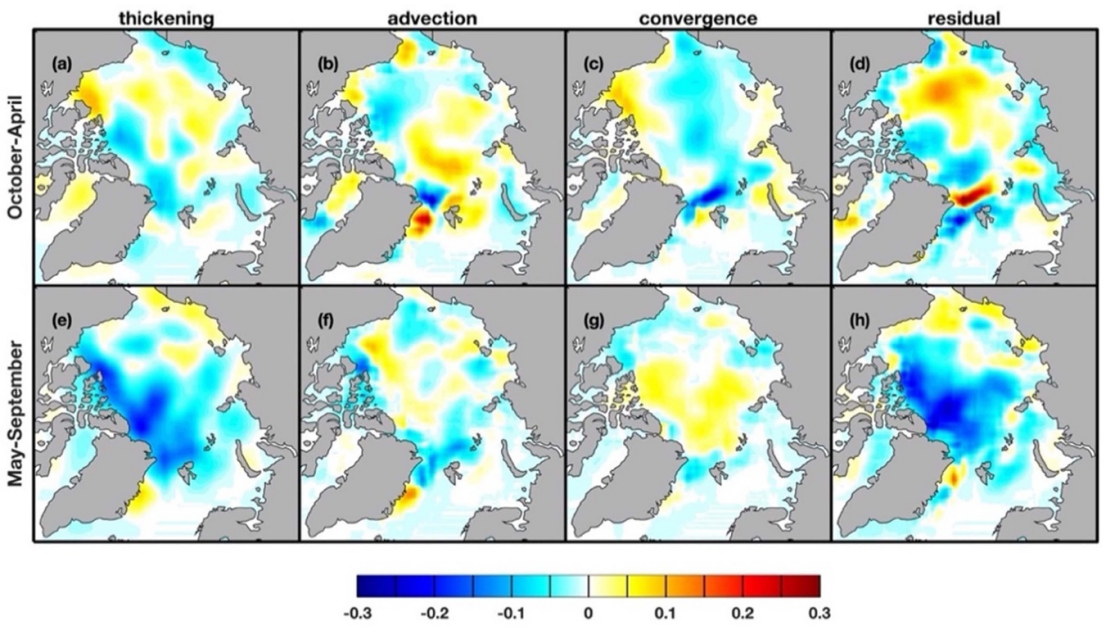


**Figure 2.** Components of the Arctic sea ice thickness budget anomalies from October 2010 to September 2011 (unit: meters per month). The panel shows the Arctic sea ice thickness budget anomalies by subtracting the six year mean (from October 2010 to September 2016) for each month. The top row (a)–(d) shows the sea ice thickness budget anomalies during sea ice advance (from October to April) and the bottom row (e)–(h) shows that during sea ice retreat (from May to September). (a), (e) thickening; (b), (f) advection; (e), (g) convergence; (d), (h) residual for each term in equation (2).

thickening anomalies through most of the Arctic, resulting in enhanced ice thickening north of the BS and CS and reduced ice thickening in ice thickness in the north of CAA. The dynamic anomalies around north and east Greenland induced residual thermodynamic changes. Increased ice advection east of Greenland caused enhanced ice melting and hence an anomalous freshwater flux to the ocean, while increased divergence north of Svalbard induced greater freezing. These changes demonstrate a stabilizing thermodynamic feedback that responds to the dynamic anomalies, as neither change is reflected in the overall ice thickening anomalies.

During the season of sea ice retreat, strong negative thickening anomalies were dominated by the residual processes, which means that the thermodynamics played a greater role in the summer ice retreat. In the regions where multi-year ice exists along the BS and CA coasts, a strong sea ice thinning is found, only very weakly offset by convergence and advection (figures 2(f) and (g)). At the same time, the mean surface net heat flux of the entire Arctic Ocean from June to August was more than the mean values from 2011 to 2016 by up to 4 W $m^{-2}$.

### 3.2. Dynamic transportation of the sea ice anomaly

The total sea ice and MYI fluxes through Fram Strait from October 2010 to September 2011 were 2282 $\pm$ 246 $km^3$ and 1830 $\pm$ 189 $km^3$, respectively (table S1). Compared with the average from 2010 to 2016, an additional 329 $km^3$ of MYI were exported through Fram Strait. During the season of ice advance, especially in October, January, March and May, ice dynamics driven by specific atmospheric circulation anomalies over the Arctic Ocean led to a significantly enhanced sea ice export through the Fram Strait (figure S4(a)). About 72% of the MYI loss was during the season of ice advance in 2011. The loss of MYI extended into the CA and the north of CAA, especially for the sea ice existing in the Arctic for more than four years (figures 3(a)–(d); supplementary figure S3). Although the data used are different, previous studies have also shown an abnormal increase in sea ice fluxes through the Fram Strait in 2011 (Ricker *et al* 2018, Min *et al* 2019). The MYI loss for the season of sea ice advance contributed to the negative summer SIT anomalies. Thus, in order to investigate the thickness anomalies in terms of ice dynamics, we assessed monthly mean NSIDC ice drift anomaly according to the export volume through the Fram Strait (figure 3).

From October to January, there was a strong and sustained negative AO phase ($-1.3$) that had not been seen since the late 1960s (Stroeve *et al* 2011). It was also found that the DA indiex showed a strong positive phase (0.68). The peak SLP anomalies (of 12 hPa) were centered east of the Arctic and gradually moved westward (figures 3(i) and (j)). In October 2010, the SLP anomalies led to a gradual convergence of sea ice from the north of the CAA toward the center of the Arctic Ocean (figures 3(e) and (i)). By January 2011, the peak SLP anomalies were centered south of Greenland. The enhanced transpolar advection transported sea ice from the

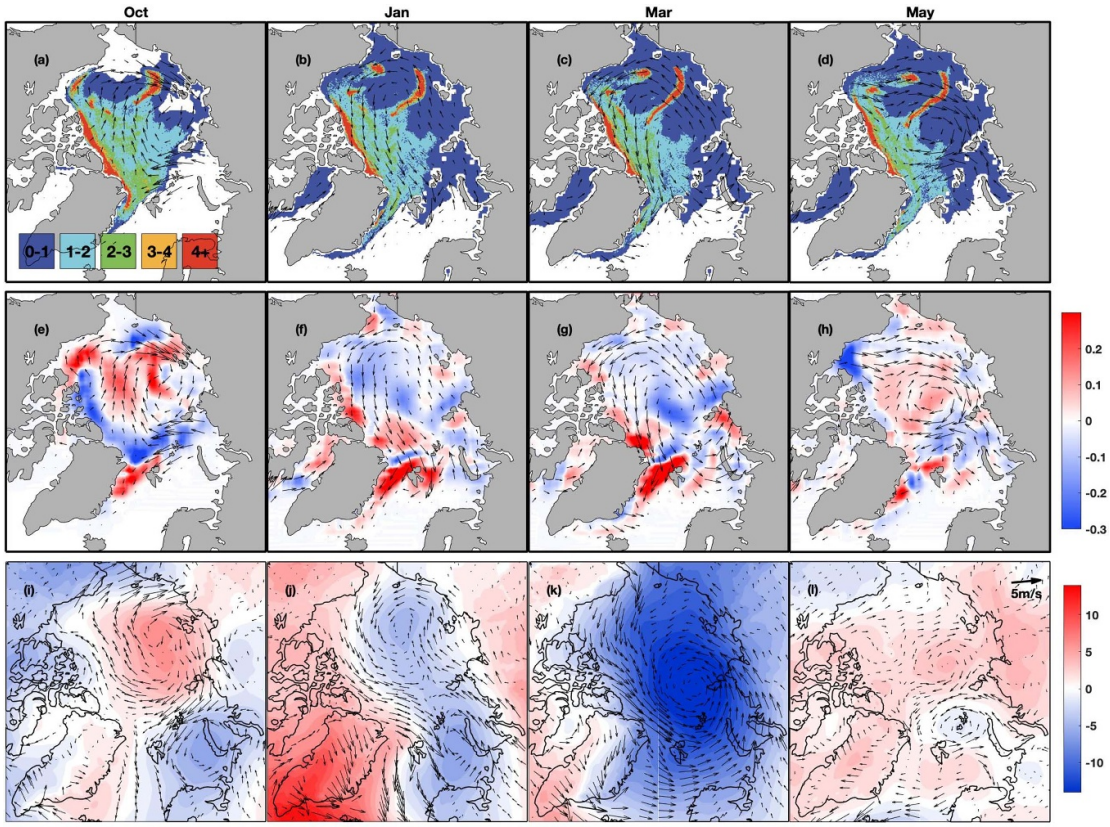


**Figure 3.** Seasonal dynamic components of Arctic sea ice thickness budget anomalies and their relation to wind forcing. Seasonal Arctic sea ice drift anomaly vector overlaid with the sea ice age (a)–(d) and the dynamic components (advection term plus convergence term: $-u\cdot\nabla H - H\nabla\cdot u$; (e)–(h) from October 2010 to May 2011. Winds velocity vector anomalies at 10 m (m $s^{-1}$) and sea level pressure anomalies (hPa) (i)–(l). Positive values indicate convergence, while negative values indicate divergence.

BS and CA to the Fram Strait (figure 3(f)). Compared with the average from October 2010 to January 2016, the amount of MYI exported through the Fram Strait increased by 219 $km^3$ from October to January (table S1).

In March, the negative SLP anomaly shifted toward the eastern Arctic Ocean, and the enhanced Transpolar Drift Stream exported an additional 116 $km^3$ of MYI through Fram Strait (table S1), contributing to the thinning of sea ice north of CAA. The positive AO weakened the Beaufort Sea High, promoting a cyclonic atmospheric circulation anomaly (figures 3(c) and (g)). Under these cyclonic surface wind anomalies, the Ekman transport deflected ice drift towards to the coast. This process decreases the recirculation of ice and increases the ice divergence over the Arctic (figure 3(g)). From 2011 February to April, the DA experienced two sharp shifts. In March, the positive DA produced a meridional wind anomaly that enhanced the Transpolar Drift Stream, exporting more ice out of the Arctic via Fram Strait. However, the surface wind anomalies decreased the Transpolar Drift Stream, leading to reduced ice transport out of the Arctic Ocean through Fram Strait in February and April.

From May to August, the AO (DA) index shifted from positive (negative) to negative (positive) phase. In May, the peak SLP anomalies (of 8 hPa) were centered over the CA, implying enhanced Ekman convergence (figure 3(k)). The Beaufort Gyre was stronger than climatological values, leading to enhanced ice transport from the south to the north Arctic and from the ESS to Fram Strait. Although the total SIV export through the Fram Strait in May 2011 did not increase significantly, the anomaly of MYI export volume in May–July 2011 was 160 $km^3$.

The relationship with the atmospheric mode and the variability of the SIV export is broadly consistent with the mechanism outlined by Wu *et al* (2006), Wang *et al* (2009), Cai *et al* (2021a, 2021b) and Wang *et al* (2021). The correlation coefficient between the DA (AO) index and the ice export anomalies was 0.58 (−0.35), reaching statistical significance at the 95% level. The DA is dynamically more important than the AO on the amount of sea ice driven out of the Arctic, because the sea ice export is dominated by the meridional wind anomaly, which is consistent with results given by Maslanik *et al* (2007b). Additionally, in March, the surface air temperature exhibited pronounced warming over the eastern Arctic, but less in the western Arctic (figure S4(d)). The positive AO and DA phase dynamically drove sea ice to be thinner, resulting in an enhanced heat flux from the ocean, while +AMO (0.15, slightly warm yr round) and

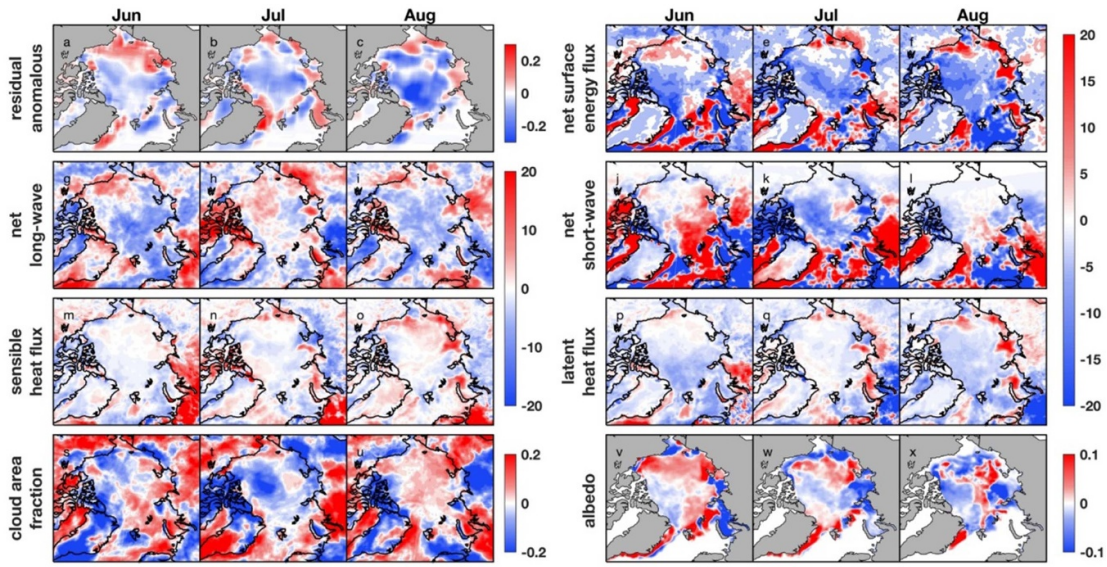


**Figure 4.** Thermodynamic residual anomalies and their relation to thermal forcing during June–August 2011. (a)–(c) The monthly thermodynamic residual anomalies (unit: meters per month) of the Arctic sea ice thickness budget in 2011 summer. (d)–(f) Surface anomalies of net energy flux; (g)–(i) net longwave radiation; (j)–(l) net shortwave radiation; m-o sensible heat fluxes; (p)–(r) latent heat flux in 2011 summer (unit: W $m^{-2}$). Shading indicates fluxes, which are positive upward. The cloud area fraction anomalies (s)–(u) and albedo anomalies (v)–(x) are denoted in bottom row.

−PDO (−1.23, very warm, yr round) were consistently warm, leading to thermodynamic melt (Rigor *et al* 2002, Cai *et al* 2021a, 2021b). The loss of MYI, together with warmer surface air temperatures, led to further loss of sea ice.

### 3.3. Thermodynamic forcing and thermodynamic feedback

Compared with the 6 year mean (from May 2011 to September 2016), the SIT budget from May to September 2011 showed a negative anomaly, indicating that the loss of SIT increased during the season of sea ice retreat, especially in the north of CAA (figure 2(e)). The spatial pattern of the thermodynamic residual anomaly was very similar to that of net surface energy flux (figures 4(a)–(f)). Persistent negative (downward) net surface energy flux anomalies were found over most parts of the negative thermodynamic residual anomalies in June-August, which was evident from figures 4(d)–(f). The net surface energy flux provided 8.67 W $m^{-2}$ more than normal values into sea ice during summer 2011 in CA.

Negative net surface longwave radiation anomalies in June were found over most of the Arctic Ocean, except the BS and CS (figure 4(g)). Anomalies of the net longwave radiation were roughly the same as those of the downward component (not shown), contributing to the energy surplus at the surface. The cloud fraction had a moderately negative anomaly in BS and CS and a positive anomaly in eastern Arctic in June (figure 4(s)). Corresponding to these anomalies in cloud amounts, these areas had strong anomalies of the downward longwave radiative forcing. In July, the reduced cloud cover over the Arctic (negative anomaly in figure 4(t)) had led to a increase in upward longwave radiation (positive anomaly in figure 4(h)). The cloud cover increased again in August, so that the downward longwave radiation was enhanced which warmed the surface.

In addition to warm Earth by reducing thermal energy loss to space, clouds can also cool the Earth by reflecting incoming sunlight to space. The net shortwave radiation showed a negative anomaly at the west of Arctic in June (figure 4(j)). The negative cloud fraction anomaly at the west of Arctic resulted in up to a 40 W $m^{-2}$ anomaly in downward shortwave radiation. Although the pattern of downward shortwave radiation (not shown) was similar to that of cloudiness, the upward shortwave radiation anomaly in the BS, CS and ESS was offset by enhanced sea ice albedo in June. In July, the negative cloud area fraction anomalies reduced the solar energy reflected to space (figure 4(t)). At the same time, the change in albedo increased the shortwave radiation absorbed, which further promoted melting and warming (figures 4(k) and (w)). In August, due to the increased cloud area fraction, the net shortwave radiation exhibited negligible positive anomalies. However, the melting of sea ice resulted in a decrease in albedo over most of the Arctic in August and contributed to an increase in net shortwave radiation absorption in CA (figures 4(x) and (l)).

The energy flux anomalies caused by net longwave and shortwave radiation were only compensated by corresponding increases of the sensible heat fluxes to a minor extent, because the surface temperature cannot increase significantly above 0 °C with ice present; the bulk of the energy went into ice melting rather than

warming of the surface. However, close to the ESS and LS the positive sensible heat flux anomalies increased (figure 4(o)) indicating that the sea surface temperature is warmer than usual.

The net surface energy flux anomalies provided extra energy, beginning in June. The net surface heat budget of the Arctic Ocean was dominated by radiative fluxes, and the exchange of heat between the Arctic Ocean and atmosphere was strongly moderated by the surface albedo, which was associated with the ice types (Perovich *et al* 2002, Perovich and Polashenski 2012, Webster *et al* 2015, Lei *et al* 2016). The correlation between the net heat flux anomalies and ice albedo in summer was 0.94, which was significant at the 95% confidence level (figure S6) as expected. Due to the significantly enhanced MYI export through the Fram Strait during the season of ice advance, once surface ice melt begins, the albedo of FYI is consistently smaller than that of MYI, resulting in more heat absorbed in the ice and transmitted to the ocean (Perovich and Polashenski 2012). From mid-June in 2011, the melt pond fraction exhibited values up to two standard deviations above the mean values for the years 2000–2011, even higher than in summer 2007 (Rösel and Kaleschke 2012). Additionally, due to the reduced cloud cover, the downward solar radiation increased, while albedo feedback further amplified the net shortwave radiation anomaly in July. Based on the investigation conducted in this paper and previous studies, more absorbed solar radiation leads to more melting and more open water, which accelerates the decline of Arctic sea ice. Both dynamical and thermodynamical forcings of teleconnection pattern can speed up the ice/ocean-albedo positive feedback loop (Perovich *et al* 2008, Cai *et al* 2021a, 2021b). Hence the loss of MYI and the anomalies of cloud fraction played significant roles, whereas the albedo anomalies acted through an amplifying feedback process when the melting was already initiated.

## 4. Summary and discussion

In this work, our study presents the thickness and volume of the Arctic Ocean ice cover from satellite observations (2003–2020), indicating there was an extreme SIT loss during 2010–2011. We quantify the SIT budget to investigate the special factors led to the precipitous decrease of SIT in 2011, using a daily SIT reanalysis data covering the melting season.

The ice thickness budget analysis suggests 81% of the ice thickness loss from 2010 to 2011 can be explained by thermodynamic forcing, while 19% of the loss is attributed to ice dynamics. Notably, the Arctic Ocean had lost 809 $km^3$ of MYI from 2010 to 2011, accounting for 88% of the total sea ice loss. About 40% of the MYI volume loss was directly due to the strengthened ice export through the Fram Strait. An extraordinarily large amount of MYI volume export through the Fram Strait during the season of sea ice advance is the important contributor to Arctic SIT and volume loss from 2010 to 2011. In terms of sea ice dynamics, the DA-associated ice drift anomalies during the season of ice advance are the major driver to the additional 233 $km^3$ of MYI transport through the Fram Strait. First-year ice, which was more sensitive to anomalies in the thermodynamic forcing, then replaced the MYI. The net decrease of SIT was partly explained by an increase in MYI export through the Fram Strait (Kwok *et al* 2009, Ryan and Münchow 2017).

Our results further demonstrate that the cloud cover exhibits a strong correlation with the thermodynamic melt of SIT. Due to the loss of MYI, the Arctic ice thickness becomes more sensitive to atmospheric anomalies in the following summer. The thermal-related Arctic SIT loss is associated with the anomalous cloudiness and enhanced downwelling net energy flux. Furthermore, the enhanced sea ice melt reduces the surface albedo, triggering a positive ice-albedo amplifying feedback and contributing to the accelerating loss of MYI. This illustrates that the increasingly younger and thinner Arctic sea ice is becoming more vulnerable to external forcing, suggesting that new record lows of Arctic sea ice extent may occur over the next few years.

Stroeve *et al* (2011) highlighted the importance of the negative winter growth feedback mechanism—thinner ice grows faster than thicker ice due to its decreased insulation. Thus, although the summer sea ice in 2011 is rapidly declining, the negative feedbacks over winter allow for recovery following low summer SIT. However, the MYI volume in October 2011 was a record low. Late-forming seasonal ice tends to be more vulnerable than MYI, which lead the Arctic sea ice more vulnerable to the storm which arrived in the central Arctic in August 2012 (Parkinson and Comiso 2013). Considering the preconditioning of Arctic ice, even without the storm, the Arctic sea ice extent might still have reached the minimum record in September 2012 (Zhang *et al* 2013). This illustrates, in the context of Arctic climate change and younger and thinner sea ice, that the Arctic sea ice is becoming more vulnerable to external forcing.

## Data availability statement

The ICESat ice thickness products from 2003 to 2008 is provided by NASA Goddard Space Flight Center (https://nsidc.org/data/NSIDC-0393/versions/1). The NASA GSFC (Goddard Space Flight Center) CryoSat-2 daily ice thickness data from October 2010 to April 2020 are available from NSIDC (https://nsidc.org/data/RDEFT4/versions/1). The AWI CryoSat-2 weekly ice thickness data on a 25km EASE2 grid are available at Meereisportal (ftp://ftp.awi.de/sea_ice/product/cryosat2). The combined Cryosat-2 and SMOS satellite data (CS2SMOS)

data from October 2010 through April 2020 is available from AWI (ftp://ftp.awi.de/sea_ice/product/cryosat2_smos). The weekly sea ice age for the Arctic Ocean is from NSIDC website (https://nsidc.org/data/NSIDC-0611/versions/4). The Arctic Oscillation (AO) index is derived from the Climate Prediction Center (CPC) (www.cpc.ncep.noaa.gov). The SLP, 10 m wind speed, surface radiation fluxes, and albedo from October 2010 to September 2016 are derived from monthly ERA5 atmospheric reanalysis data from the European Centre for Medium-Range Weather Forecasts (ECMWF; https://cds.climate.copernicus.eu/cdsapp#!/dataset/reanalysis-era5-single-levels-monthly-means?tab?form).

The data that support the findings of this study are available upon reasonable request from the authors.

## Acknowledgments

This work was supported by the National Natural Science Foundation of China (Nos. 42106233, 41922044, 41941009, 41676185 and 42106226), the Southern Marine Science and Engineering Guangdong Laboratory (Zhuhai) (No. SML2020SP007), the Guangdong Basic and Applied Basic Research Foundation (No. 2020B1515020025), the State Key Laboratory of Cryospheric Science (No. SKLCS-OP-2020-3), the China Postdoctoral Science Foundation (No. 2020M683022) and the fundamental research funds for the Norges Forskningsråd. (No. 328886). We thank two anonymous reviewers for their helpful comments which improved the paper. We acknowledge the WMO WWRP for its role in coordinating this international research activity. This is a contribution to the Year of Polar Prediction (YOPP), a flagship activity of the Polar Prediction Project (PPP), initiated by the World Weather Research Programme (WWRP) of the World Meteorological Organisation (WMO).

## Conflict of interest

None declared.

## ORCID iDs

Xuewei Li https://orcid.org/0000-0003-3435-7422
Chao Min https://orcid.org/0000-0002-4181-2107

## References

Bitz C M, Holland M M, Hunke E C and Moritz R E 2005 Maintenance of the sea-ice edge *J. Clim.* **18** 2903–21

Cai Q, Beletsky D, Wang J and Lei R 2021a Interannual and decadal variability of Arctic summer sea ice associated with atmospheric teleconnection patterns during 1850–2017 *J. Clim.* **34** 9931–55

Cai Q, Wang J, Beletsky D, Overland J, Ikeda M and Wan L 2021b Accelerated decline of summer Arctic sea ice during 1850–2017 and the amplified Arctic warming during the recent decades *Environ. Res. Lett.* **16** 034015

Comiso J C 2002 A rapidly declining perennial sea ice cover in the Arctic *Geophys. Res. Lett.* **29** 17.1–4

Copernicus Climate Change Service (C3S) 2017 ERA5: fifth generation of ECMWF atmospheric reanalyses of the global climate *Copernicus Climate Change Service Climate Data Store (CDS)* (Accessed 4 May 2018)

Hersbach H *et al* 2020 The ERA5 global reanalysis *Q. J. R. Meteorol. Soc.* **146** 1999–2049

Holland P R, Bruneau N, Enright C, Losch M, Kurtz N T and Kwok R 2014 Modeled trends in antarctic sea ice thickness *J. Clim.* **27** 3784–801

Holland P R and Kimura N 2016 Observed concentration budgets of Arctic and Antarctic sea ice *J. Clim.* **29** 5241–9

Krumpen T, Gerdes R, Haas C, Hendricks S, Herber A, Selyuzhenok V, Smedsrud L and Spreen G 2016 Recent summer sea ice thickness surveys in Fram Strait and associated ice volume fluxes *Cryosphere* **10** 523–34

Kurtz N and J Harbeck 2017 CryoSat-2 Level-4 Sea Ice Elevation, Freeboard, and Thickness, Version 1 (NASA National Snow and Ice Data Center Distributed Active Archive Center) (https://doi.org/10.5067/96JO0KIFDAS8)

Kwok R and Cunningham G F 2015 Variability of arctic sea ice thickness and volume from CryoSat-2 *Phil. Trans. R. Soc.* A **373** 20140157

Kwok R, Cunningham G F, Wensnahan M, Rigor I, Zwally H J and Yi D 2009 Thinning and volume loss of the Arctic Ocean sea ice cover: 2003–2008 *J. Geophys. Res.* **114** 2003–8

Kwok R and Rothrock D A 2009 Decline in Arctic sea ice thickness from submarine and ICESat records: 1958–2008 *Geophys. Res. Lett.* **36** L15501

Kwok R and Untersteiner N 2011 The thinning of Arctic sea ice *Phys. Today* **64** 36–41

Lei R, Tian-Kunze X, Leppäranta M, Wang J, Kaleschke L and Zhang Z 2016 Changes in summer sea ice, albedo, and portioning of surface solar radiation in the Pacific sector of Arctic Ocean during 1982–2009 *J. Geophys. Res.* **121** 5470–86

Liu Y, Key J R, Wang X and Tschudi M 2020 Multidecadal Arctic sea ice thickness and volume derived from ice age *Cryosphere* **14** 1325–45

Maslanik J A, Fowler C, Stroeve J, Drobot S, Zwally J, Yi D and Emery W 2007a A younger, thinner Arctic ice cover: increased potential for rapid, extensive sea-ice loss *Geophys. Res. Lett.* **34** 2004–8

Maslanik J, Drobot S, Fowler C, Emery W and Barry R 2007b On the Arctic climate paradox and the continuing role of atmospheric circulation in affecting sea ice conditions *Geophys. Res. Lett.* **34** 2–5

Maslanik J, Stroeve J, Fowler C and Emery W 2011 Distribution and trends in Arctic sea ice age through spring 2011 *Geophys. Res. Lett.* **38** 2–7

McPhee M G, Stanton T P, Morison J H and Martinson D G 1998 Freshening of the upper ocean in the Arctic: is perennial sea ice disappearing? *Geophys. Res. Lett.* **25** 1729–32

Min C, Mu L, Yang Q, Ricker R, Shi Q, Han B, Wu R and Liu J 2019 Sea ice export through the Fram Strait derived from a combined model and satellite data set *Cryosphere* **13** 3209–24

Mu L, Losch M, Yang Q, Ricker R, Losa S N and Nerger L 2018 Arctic-wide sea ice thickness estimates from combining satellite remote sensing data and a dynamic ice-ocean model with data assimilation during the CryoSat-2 period *J. Geophys. Res.* **123** 7763–80

Parkinson C L and Comiso J C 2013 On the 2012 record low Arctic sea ice cover: Combined impact of preconditioning and an August storm *Geophys. Res. Lett.* **40** 1356–61

Perovich D K, Grenfell T C, Light B and Hobbs P V 2002 Seasonal evolution of the albedo of multiyear Actic sea ice *J. Geophys. Res.* **107** SHE–20

Perovich D K and Polashenski C 2012 Albedo evolution of seasonal Arctic sea ice *Geophys. Res. Lett.* **39** L08501

Perovich D K, Richeter-Menge J A, Jones K F and Light B 2008 Sunlight, water, and ice: extreme Arctic sea ice melt during the summer of 2007 *Geophys. Res. Lett.* **35** 2–5

Ricker R, Girard-Ardhuin F, Krumpen T and Lique C 2018 Satellite-derived sea ice export and its impact on Arctic ice mass balance *Cryosphere* **12** 3017–32

Ricker R, Hendricks S, Helm V, Skourup H and Davidson M 2014 Sensitivity of CryoSat-2 Arctic sea-ice freeboard and thickness on radar-waveform interpretation *Cryosphere* **8** 1607–22

Rigor I G, Wallace J M and Colony R L 2002 Response of sea ice to the Arctic oscillation *J. Clim.* **15** 2648–63

Rösel A and Kaleschke L 2012 Exceptional melt pond occurrence in the years 2007 and 2011 on the Arctic sea ice revealed from MODIS satellite data *J. Geophys. Res.* **117** 1–8

Rothrock D A, Percival D B and Wensnahan M 2008 The decline in arctic sea-ice thickness: separating the spatial, annual, and interannual variability in a quarter century of submarine data *J. Geophys. Res.* **113** 1–9

Ryan P A and Münchow A 2017 Sea ice draft observations in Nares Strait from 2003 to 2012 *J. Geophys. Res.* **122** 3057–80

Screen J A, Simmonds I and Keay K 2011 Dramatic interannual changes of perennial Arctic sea ice linked to abnormal summer storm activity *J. Geophys. Res.* **116**

Stroeve J C, Maslanik J, Serreze M C, Rigor I, Meier W and Fowler C 2011 Sea ice response to an extreme negative phase of the Arctic oscillation during winter 2009/2010 *Geophys. Res. Lett.* **38** 1–6

Tilling R L, Ridout A, Shepherd A and Wingham D J 2015 Increased Arctic sea ice volume after anomalously low melting in 2013 *Nat. Geosci.* **8** 643–6

Tschudi M A, Meier W N and Scott Stewart J 2020 An enhancement to sea ice motion and age products at the national snow and ice data center (NSIDC) *Cryosphere* **14** 1519–36

Wang J, Zhang J, Watanabe E, Ikeda M, Mizobata K, Walsh J E, Bai X and Wu B 2009 Is the dipole anomaly a major driver to record lows in arctic summer sea ice extent? *Geophys. Res. Lett.* **36** 1–5

Wang Q, Ricker R and Mu L 2021 Arctic sea ice decline preconditions events of anomalously low sea ice volume export through fram strait in the early 21st century *J. Geophys. Res.* **126** 1–14

Webster M A, Rigor I G, Perovich D K, Richter-Menge J A, Polashenski C M and Light B 2015 Seasonal evolution of melt ponds on Arctic sea ice *J. Geophys. Res.* **120** 5968–82

Wu B, Wang J and Walsh J E 2006 Dipole anomaly in the winter Arctic atmosphere and its association with sea ice motion *J. Clim.* **19** 210–25

Zhang J, Lindsay R, Schweiger A and Steele M 2013 The impact of an intense summer cyclone on 2012 Arctic sea ice retreat *Geophys. Res. Lett.* **40** 720–6